J Eng Math
DOI 10.1007/s10665-007-9193-z

# Acoustic scattering at a hard–soft lining transition in a flow duct


**Sjoerd W. Rienstra**

Received: 5 January 2007 / Accepted: 27 August 2007


**Abstract** An explicit Wiener–Hopf solution is derived to describe the scattering of sound at a hard–soft wall impedance transition at $x = 0$, say, in a circular duct with uniform mean flow of Mach number $M$. A mode, incident from the upstream hard section, scatters at $x = 0$ into a series of reflected modes and a series of transmitted modes. Of particular interest is the role of a possible instability along the lined wall in combination with the edge singularity. If one of the "upstream" running modes is to be interpreted as a downstream-running instability, an extra degree of freedom in the Wiener–Hopf analysis occurs that can be resolved by application of some form of Kutta condition at $x = 0$, for example a more stringent edge condition where wall streamline deflection $h = \mathcal{O}(x^{3/2})$ at the downstream side. In general, the effect of this Kutta condition is significant, but it is particularly large for the plane wave at low frequencies and should therefore be easily measurable. For small Helmholtz numbers, the reflection coefficient modulus $|R_{001}|$ tends to $(1 + M)/(1 - M)$ without and to 1 with Kutta condition, while the end correction tends to $\infty$ without and to a finite value with Kutta condition. This is exactly the same behaviour as found for reflection at a pipe exit with flow, irrespective if this is uniform or jet flow. Although the presence of the instability in the model is hardly a question anymore since it has been confirmed numerically, a proper mathematical causality analysis is still not totally watertight. Therefore, the limit of a vortex sheet, separating zero flow from mean flow, approaching the wall has been explored. Indeed, this confirms that the Helmholtz unstable mode of the free vortex sheet transforms into the suspected mode and remains unstable. As the lined-wall vortex-sheet model predicts unstable behaviour for which experimental evidence is at best rare and indirect, the question may be raised if this model is indeed a consistent simplification of reality, doing justice to the double limit of small perturbations and a thin boundary layer. Numerical time-domain methods suffer from this instability and it is very important to decide whether the instability is at least physically genuine. Experiments based on the present problem may provide a handle to resolve this stubborn question.

**Keywords** Aircraft noise · Duct acoustics · Impedance models · Wiener–Hopf method

S. W. Rienstra (✉)
Department of Mathematics and Computer Science, Eindhoven University of Technology, P.O. Box 513, 5600 MB, Eindhoven, The Netherlands
e-mail: s.w.rienstra@tue.nl

## 1 James Lighthill and aero-acoustics

James Lighthill's involvement with aero-acoustics is legendary [1,2]. As far as aero-acoustics regards the generation of sound by aerodynamic disturbances (turbulence), Lighthill defined aero-acoustics. With the publication of his most influential first paper [3] on the subject, certainly acoustics suddenly gained a higher profile. In contrast to modern aero-acoustics [4], sound was barely considered to be a fluid-mechanical phenomenon. The coupling of sound with flow was restricted to advection, and nobody knew how sound was generated by unsteady flow. In this first paper Lighthill showed by refined mathematical analysis and brilliant scaling arguments that the far field intensity (averaged energy flux) of sound produced by (compact, cold, low-subsonic) turbulent eddies (the most inefficient type of source) is proportional to $U^8$, where $U$ is the typical mean flow speed. It goes without saying that this paper opened a new discipline and produced an enormous amount of research and insight after it [5–7], even in unexpected areas like gravity and acoustic waves brought about by turbulence in the atmosphere of the sun [8]. A very readable review is still Crighton's [9]. The latest developments can be found in Howe [10].

Remarkably, before Lighthill's publications most reports of measured noise data gave a $U^4$ variation, whereas after it only the 8th power dependence was recognised to be correct, the 4th power being associated to other noise sources [11]. It just goes to show how practical a good theory is.

This high power of the mean flow gave the aircraft engine engineers of the 1950s a second reason to reduce the jet speed by equipping the jet engine with a turbofan and bypass duct [12]. The first one was of course the greater fuel efficiency that is obtained by reducing the energy flux through a cross-section $A$ ($\sim \rho U^3 A$) by increasing $A$ and decreasing $U$ such that the thrust ($\sim \rho U^2 A$) is fixed.

The resulting *turbofan revolution* of increased by-pass ratios, which started in the 1960s and still continues, controlled jet noise to an extent that the interaction noise of fan and stator became dominant. This required research on the propagation of sound in ducts and sheared mean flow. Lighthill was of course fully aware of that, as he promoted study of this subject directly [13] and indirectly [14].

A central issue for the interpretation of duct modes is the question of their direction of propagation. If we know for certain that a mode decays, either because it is cut off (carrying no energy at all) or because it is damped (energy is dissipated), this question is relatively easily answered by the direction of decay. When the mode propagates unattenuated, we have to invoke more subtle arguments based on the direction of group velocity [15] or causal arguments based on analyticity in the complex frequency, which for the easier cases of real axial wavenumbers was translated by Lighthill [16,17] into an argument[1] of a *slowly increasing* source strength $\sim \mathrm{e}^{\mathrm{i}\omega t+\varepsilon t}$. If the axial wavenumber is not real, the mode is either damped or exponentially unstable (depending on the direction we can associate to it), and we have a more serious problem.

Inspired by these ideas of Lighthill, we will consider a problem that originates from the topic of aircraft engine-duct acoustics. It deals with sound interacting with the vortical boundary layer—in the limit of a vortex sheet—along a lined wall and pursues the question of a possible instability.

## 2 Introduction

### 2.1 Duct modes and boundary conditions

The sound field in a lined duct with flow may be written as an infinite sum of modes if geometry, lining and mean flow are independent of the axial coordinate. Mathematically, modes form a complete basis for the representation of the sound field but, physically, they are each also (self-similar) solutions of the equations. Therefore, they provide much insight into the physical behaviour of the sound propagation. Most of our knowledge of duct acoustics is based on understanding the modes. Even for ducts with slowly varying cross-section the concept of modes is applicable through the WKB *ansatz* of negligible intermodal interaction [18,19].

[1] Of course, closely related to the older argument of adding a small amount of damping by assuming the sound speed slightly complex.

The configuration that we will consider here is a circular duct of constant cross-section, uniform mean flow and an acoustically soft, locally reacting wall, which can be described in the frequency domain by an impedance. This simple but relevant model has served for years in industry to optimise the design of aircraft-engine liners [20].

A fundamental problem in the modelling of a lined wall with uniform mean flow is the limiting form of the impedance boundary condition when the boundary layer becomes much thinner than an acoustic wavelength. The presently accepted Ingard–Myers boundary condition was originally proposed by Ingard [21] for a plane wall and later generalised by Myers [22] for curved walls. It adopts the point of view of concentrating the vorticity of the boundary layer in a vortex sheet very close but not at the wall, such that the boundary condition at the wall and the continuity conditions across the vortex sheet can be applied without conflict. The asymptotic analysis by Eversman and Beckemeyer [23] of the limit of a continuous profile with vanishing boundary layer, yields the same condition, with the proviso that they avoided the critical layer and assumed the mean flow velocity nowhere being equal to the modal phase velocity. Nevertheless it is clear that the small boundary-layer thickness and the small perturbation amplitudes involve a double limit which may be non-uniform, possibly calling for nonlinear or other conditions.

The modes in lined circular ducts with uniform mean flow are rather well understood [24]. With hard walls we have a finite number of cut-on (axially propagating) and infinitely many cut-off (axially exponentially decaying) modes. With soft walls[2] this difference is slightly blurred; all modes decay exponentially but some are weakly cut-off while the others are heavily cut-off. Apart from this difference in axial direction, there is also a marked difference in the cross-wise (radial) direction. Most modes are present throughout the duct, but some exist only near the wall. They decay exponentially in the radial direction away from the wall. These modes are called surface waves. Some exist both with and without flow, but some only with mean flow (of either type at most two per circumferential order for a hollow duct, four for an annular duct). The ones that exist only with mean flow are thus called hydrodynamic surface waves [24].

### 2.2 Instability waves

By analogy with the Helmholtz instability along an interface between two media of different velocities, the possibility was raised by Tester [25] that one such hydrodynamic surface wave may have the character of an instability. This means that the mode may seem to propagate in the upstream direction if the exponential decay is followed, but in reality its direction of propagation is downstream while it increases exponentially. Tester [25] verified this conjecture by the causality argument of Briggs and Bers [26–28] (using physically reasonable frequency dependent impedance models) and found that the suspected surface wave indeed may be an instability, at least according to the Briggs–Bers formalism. This was confirmed analytically by Rienstra [24] for an incompressible limit of waves along an impedance of mass-spring-damper type, but now using the related causality criterion of Crighton and Leppington [29,30].

In order to avoid the instability problem, Quinn and Howe [31] studied the scattering of sound at a lossless liner's leading edge (impedance zero). In this case the only neutrally unstable hydrodynamic surface waves are convected by the mean flow. They found qualitatively the same effects as for the airfoil trailing edge [32].

Extending these ideas, Koch and Möhring [33] analysed by a generalised Wiener–Hopf solution the scattered sound field in a 2D duct with mean flow and a *finite* lined section. They allowed for possible instabilities, although their (Briggs–Bers) causality analysis was incomplete because they considered only frequency *in*dependent impedances, which in general cannot exist. They concluded that without instability wave available, the liner's leading-edge singularity could be no less than rather strong (i.e., corresponding to a singular velocity field). If there is an instability, this singularity can be weak, similar to the Kutta condition for a trailing edge.[3] The singularity at the liner's trailing edge is more difficult to model [35,36] (the proper modelling may well be a nonlinear one and involve

[2] Note that 'soft wall' means throughout 'wall of finite impedance', not 'pressure-release wall'.

[3] This Kutta condition essentially results from a delicate balance between viscous effects, nonlinear inertia and acceleration, described by a form of triple-deck theory [32,34]. It would be of interest to investigate if any consistent high-Reynolds triple deck or other structure is possible that is compatible with no instability and no Kutta condition.

essentially a finite-thickness mean flow boundary layer) and the scattering by this edge may add a certain amount of uncertainty to the results. This, however, is greatly overshadowed by the fact that the field obtained in the lined section becomes exponentially large when the instability is included. This is in the greatest contrast with the usual experience in industry [20].

For a part, this may be explained by the fact that a typical liner's impedance has a dimensionless real part (resistance) of the order of unity or larger. For much smaller resistances, Ronneberger [37] and Aurégan et al. [38] found for sound waves propagating through ducts with a finite lined section considerable amplifications when mean flow is present. Both authors suggest that this phenomenon may be explained by instability waves in the lined section, thus yielding at least an indirect proof of the existence of these waves. (Note that none of these authors compared their results with [33].)

It is therefore still an open question if these modes are always or only sometimes unstable, or maybe essentially nonlinear for any reasonable acoustic amplitude because of the very high amplification rate.

On the other hand, this is not very unlike the situation for a free-stream jet. In agreement with theory, an instability indeed starts off the exit edge; however, further downstream the predicted Helmholtz instability is much less than is observed, because it quickly reaches the nonlinear regime. Still the major predicted acoustic consequences due to the excitation of the instability are very well described by linear theory [29,39–52] and it makes sense to investigate a common situation.

In the jet-exit problem we know that the instability may be excited by vortex shedding from a sharp edge. In the inviscid models we are dealing with, the vortex shedding is enforced by application of the Kutta condition [34,49]. By analogy we propose here the canonical problem of a duct, consisting of a semi-infinite hard-walled section and a semi-infinite lined section, with a mean flow that runs from the hard-walled to the soft-walled parts. The liner instability, if available, will be excited by application of some form of Kutta condition. We deliberately consider a simpler geometry than Koch and Möhring [33], in order to achieve more analytical results and to isolate the liner's leading-edge effects from any trailing-edge effects.

We will show that in the low-Helmholtz-number limit there results a very large acoustical difference between presence and absence of the instability. In similar problems for the exhaust jet it has been shown experimentally that the excitation of an instability is really physical and the effect on the acoustics is just as big as the theory predicts [42,44–47,52].

### 2.3 Causality conditions

Rather than the Briggs–Bers criterion (BB) we will use the Crighton–Leppington [29,30] causality test (CL), because BB is not applicable to Helmholtz-type instabilities. It requires the system to have a maximum temporal growth rate for all real wavenumbers. Such a maximum exists for free shear layers of finite thickness [53]—or more precisely: a maximum Strouhal number based on the shear layer thickness—and there is probably one for a finite boundary layer along a lined wall, but this is as yet unknown. With Helmholtz instabilities along vortex sheets of zero thickness the growth rate is not bounded since the axial wavenumber is asymptotically linearly proportional to the frequency. It may be true that the validity of the CL test in a stricter sense has been proved mathematically by Jones and Morgan [54], but since this proof relies on the rather exotic concept of ultradistribution, it is far from certain that there exists a one-to-one correspondence in all its conclusions between the model and the modelled physical phenomena; for example, because of the several non-uniform limits involved.

Therefore, we will use the CL test to identify the suspicious mode in question, but with reservation, and in order to augment the credibility of the conclusion this test will be aided by a separate analysis of the behaviour of these modes for a configuration of the vortex sheet set at a finite distance off the wall.

### 2.4 Wiener–Hopf

Although the present problem might be solved for most practical engineering purposes in a satisfactory way by mode matching, this method is not useful here as it provides (in its direct form) no control of the edge singularity

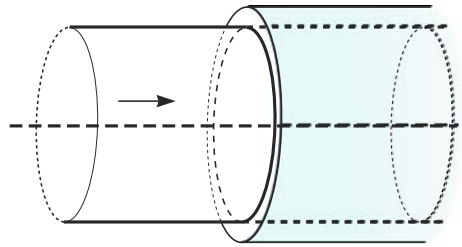

**Fig. 1** Sketch of geometry

other than a posteriori by checking the convergence rate of the modal amplitudes. A much better approach in this respect is the Wiener–Hopf technique [55]. The problem of sound scattered in a semi-infinite duct is very apt to be treated by this method, while the edge singularity plays a most prominent role via the order of a polynomial function.

The pioneering Wiener–Hopf solution by Heins and Feshbach [56] without flow is almost as classical as the related problem for the unflanged pipe exit by Levine and Schwinger [57], but we will not follow their approach. To include flow and Kutta condition in a convenient way, we will use a 3D version of the 2D analysis outlined in [58].

## 3 The problem

We assume a steady-state motion, and adopt an $\mathrm{e}^{\mathrm{i}\omega t}$-sign convention, while the exponent is dropped throughout for brevity. Consider the problem of the scattering of duct modes at a hard–soft wall-impedance transition in a circular duct of radius $a$ with uniform mean flow velocity $U_0$, density $\rho_0$ and soundspeed $c_0$ (see Fig. 1). Following [24] we make dimensionless: lengths on $a$, time on $a/c_0$, velocities on $c_0$, densities on $\rho_0$, and pressures on $\rho_0 c_0^2$. Noting that in uniform flow pressure, vorticity and entropy perturbations are decoupled, we leave vorticity and entropy perturbations unspecified and consider only the pressure field.

In particular, we have in a circular duct $r = 1, -\infty < x < \infty$ with uniform mean flow Mach number $M = U_0/c_0 > 0$ and a hard wall along $x < 0$ and a wall of impedance $Z$ along $x > 0$. The time-harmonic acoustic field, with frequency $\omega > 0$, satisfies

$$\left(\mathrm{i}\omega + M\frac{\partial}{\partial x}\right)^2 p - \nabla^2 p = 0, \tag{1a}$$

$$\left(\mathrm{i}\omega + M\frac{\partial}{\partial x}\right)\boldsymbol{v} + \nabla p = 0, \tag{1b}$$

with Ingard–Myers boundary conditions [21,22] along $r = 1$

$$x < 0: \quad (\boldsymbol{v}\cdot\boldsymbol{e}_r) = 0, \tag{2a}$$

$$x > 0: \quad \mathrm{i}\omega Z(\boldsymbol{v}\cdot\boldsymbol{e}_r) = \left(\mathrm{i}\omega + M\frac{\partial}{\partial x}\right)p, \tag{2b}$$

(which is essentially just the impedance condition along the wall modified by a form of Snell's law to allow for refraction by the wall boundary layer), while the field is regular at all points in the interior of the duct. Note that $Z = Z(\omega)$ in some physically suitable way. Assume the incident (i.e., right-running) mode in the hard-walled part $x < 0$

$$p_{\mathrm{in}} = \mathrm{J}_m(\alpha_{m\mu} r)\,\mathrm{e}^{-\mathrm{i}m\theta - \mathrm{i}\kappa_{m\mu} x}, \tag{3}$$

where circumferential mode number $m \geqslant 0$ and $\mathrm{J}_m$ is the $m$th order ordinary Bessel function of the first kind [59]. Here, $-\alpha_{m\mu}^2$ is an eigenvalue of the Laplace operator in a circular cross-section with Neumann boundary conditions, and given by

$$\alpha_{m\mu}^{1-m}\,\mathrm{J}'_m(\alpha_{m\mu})=0, \tag{4}$$

i.e., the non-trivial zeros of $\mathrm{J}'_m$. The quantity $\alpha_{m\mu}$ is usually called the radial modal wavenumber. The axial modal wavenumber $\kappa_{m\mu}$ is defined through the dispersion relation

$$\alpha_{m\mu}^2+\kappa_{m\mu}^2=(\omega-M\kappa_{m\mu})^2 \tag{5}$$

such that the branch is taken with $\mathfrak{Re}(\kappa_{m\mu})>0$ if the mode is cut-on or $\mathfrak{Im}(\kappa_{m\mu})<0$ if the mode is cut-off. Due to circumferential symmetry, the scattered wave will depend on $\theta$ via $\mathrm{e}^{-\mathrm{i}m\theta}$ only, and we will from here on assume that $p:=p\,\mathrm{e}^{-\mathrm{i}m\theta}$ where the exponent will be dropped.

After introducing the velocity potential with $\boldsymbol{v}=\nabla\phi$, we can integrate (1b) to get

$$\Big(\mathrm{i}\omega+M\frac{\partial}{\partial x}\Big)\phi+p=0. \tag{6}$$

(The integration constant is not important.) So we have for the corresponding incident mode

$$\phi_{\mathrm{in}}=\frac{\mathrm{i}}{\omega-M\kappa_{m\mu}}p_{\mathrm{in}}. \tag{7}$$

We introduce the scattered part $\psi$ of the potential by

$$\phi=\phi_{\mathrm{in}}+\psi. \tag{8}$$

It is convenient to reformulate the boundary condition by way of the wall streamline given by

$$r=1+\mathfrak{Re}\big(h(x)\,\mathrm{e}^{\mathrm{i}\omega t-\mathrm{i}m\theta}\big), \tag{9}$$

Of course, the wall streamline is not really positioned at the wall (which is not porous in the axial direction) but taken in the limit of approaching the wall. Then the acoustic velocity between the wall streamline and the wall is uniform in the radial direction, and thus given by $\mathrm{i}\omega h$. Furthermore, the acoustic pressure is here also uniform radially, and, being continuous across the streamline, equal to the wall pressure in the mean flow. We have then at $r=1$ (note that $\partial\phi_{\mathrm{in}}/\partial r=0$ at $r=1$)

$$\frac{\partial\psi}{\partial r}=0\quad\text{for } x<0, \tag{10a}$$

$$\frac{\partial\psi}{\partial r}=\Big(\mathrm{i}\omega+M\frac{\partial}{\partial x}\Big)h\quad\text{for } x>0, \tag{10b}$$

$$p=\mathrm{i}\omega Zh\quad\text{for } x>0. \tag{10c}$$

We expect some singular behaviour at $x=0$, but no more than what goes together with a continuous wall streamline, so $h(0)=0$ and $h(x+)\leqslant\mathcal{O}(x^\eta)$ for a $\eta>0$.

## 4 The Wiener–Hopf analysis

We introduce the Fourier transforms to $x$

$$\hat{\psi}(\kappa, r) = \int_{-\infty}^{\infty} \psi(x, r)\, \mathrm{e}^{\mathrm{i}\kappa x}\, \mathrm{d}x, \tag{11a}$$

$$H_+(\kappa) = \int_{0}^{\infty} h(x)\, \mathrm{e}^{\mathrm{i}\kappa x}\, \mathrm{d}x, \tag{11b}$$

$$P_-(\kappa) = \int_{-\infty}^{0} \Big(\mathrm{i}\omega + M\frac{\partial}{\partial x}\Big)\psi(x, 1)\, \mathrm{e}^{\mathrm{i}\kappa x}\, \mathrm{d}x, \tag{11c}$$

to obtain for $\hat{\psi}$ the Bessel-type equation

$$\frac{\partial^2\hat{\psi}}{\partial r^2} + \frac{1}{r}\frac{\partial\hat{\psi}}{\partial r} + \left[(\omega - M\kappa)^2 - \kappa^2 - \frac{m^2}{r^2}\right]\hat{\psi} = 0. \tag{12}$$

We introduce the reduced frequency $\Omega$, Fourier wavenumber $\sigma$ and radial wavenumber $\gamma$ as follows

$$\begin{aligned} &\beta = \sqrt{1 - M^2}, \quad \omega = \beta\Omega, \quad \kappa = \frac{\Omega}{\beta}(\sigma - M), \\ &\Omega\gamma = \sqrt{(\omega - M\kappa)^2 - \kappa^2} = \Omega\sqrt{1 - \sigma^2}, \\ &\gamma = \sqrt{1 - \sigma^2} \quad \text{where } \Im\mathrm{m}(\gamma) \leqslant 0. \end{aligned} \tag{13}$$

With (10a), (10b) and (11b) we arrive at the solution

$$\hat{\psi} = A(\sigma)\, \mathrm{J}_m(\Omega\gamma r), \tag{14a}$$

$$A(\sigma) = \mathrm{i}\frac{1 - M\sigma}{\beta\gamma\, \mathrm{J}'_m(\Omega\gamma)}H_+. \tag{14b}$$

Since

$$\Big(\mathrm{i}\omega + M\frac{\partial}{\partial x}\Big)\psi = p_{\mathrm{in}} - p, \tag{15}$$

we have along the wall $r = 1$:

$$\mathrm{i}(\omega - M\kappa)A\, \mathrm{J}_m(\Omega\gamma) = P_- + \int_0^{\infty} p_{\mathrm{in}}\, \mathrm{e}^{\mathrm{i}\kappa x}\, \mathrm{d}x - \int_0^{\infty} p\, \mathrm{e}^{\mathrm{i}\kappa x}\, \mathrm{d}x, \tag{16}$$

which reduces to

$$\mathrm{i}(\omega - M\kappa)A\, \mathrm{J}_m(\Omega\gamma) = P_- + \frac{\mathrm{i}\, \mathrm{J}_m(\alpha_{m\mu})}{\kappa - \kappa_{m\mu}} - \mathrm{i}\omega Z H_+, \tag{17}$$

and

$$-\frac{\Omega}{\beta^2}(1 - M\sigma)^2\frac{\mathrm{J}_m(\Omega\gamma)}{\gamma\, \mathrm{J}'_m(\Omega\gamma)}H_+ + \mathrm{i}\beta\Omega Z H_+ = P_- + \frac{\mathrm{i}\beta\, \mathrm{J}_m(\alpha_{m\mu})}{\Omega(\sigma - \sigma_{m\mu})}, \tag{18}$$

where we introduced

$$\sigma_{m\mu} = \sqrt{1 - \frac{\alpha_{m\mu}^2}{\Omega^2}}, \tag{19}$$

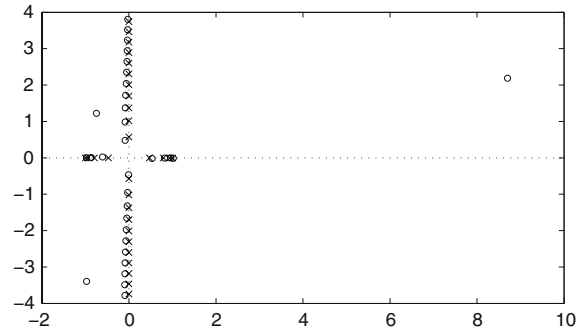


**Fig. 2** Typical location of soft-wall wavenumbers $\tau_{m\nu}$ (indicated by ○) and hard-wall wavenumbers $\sigma_{m\nu}$ (indicated by ×). Note the three soft-wall surface waves ($Z = 0.8 - 2\mathrm{i}$, $\omega = 10$, $M = 0.5$, $m = 0$)

such that $\mathfrak{Re}(\sigma_{m\mu}) > 0$ and $\mathfrak{Im}(\sigma_{m\mu}) = 0$, or $\mathfrak{Im}(\sigma_{m\mu}) < 0$. This yields

$$P_-(\sigma) + \frac{\mathrm{i}\beta\,\mathrm{J}_m(\alpha_{m\mu})}{\Omega(\sigma - \sigma_{m\mu})} = -K(\sigma)H_+(\sigma), \tag{20}$$

where the Wiener–Hopf kernel $K$ is defined by

$$K(\sigma) = \frac{\Omega}{\beta^2}(1 - M\sigma)^2 \frac{\mathrm{J}_m(\Omega\gamma)}{\gamma\,\mathrm{J}'_m(\Omega\gamma)} - \mathrm{i}\beta\Omega Z. \tag{21}$$

Note that $\mathrm{J}_m(\Omega\gamma)/\Omega\gamma\,\mathrm{J}'_m(\Omega\gamma)$ is a meromorphic function of $\Omega^2\gamma^2$ and therefore of $\sigma^2$. So $K$ is a meromorphic function of $\sigma$ with isolated poles and zeros. The zeros, corresponding with the reduced axial wavenumbers in the lined part of the duct, are given by

$$\chi(\sigma) = (1 - M\sigma)^2\,\mathrm{J}_m(\Omega\gamma) - \mathrm{i}\beta^3 Z\gamma\,\mathrm{J}'_m(\Omega\gamma) = 0 \tag{22}$$

and denoted by $\sigma = \tau_{m\nu}$, $\nu = 1, 2, \ldots$, for the right-running modes of the lower complex halfplane (see Fig. 2). The only[4] possible candidate of a right-running mode from the upper half-plane (which then has to be an instability) will be denoted (following [24]) by $\sigma = \sigma_{HI}$, where the subscript refers to "hydrodynamic instability" (a possible example is found in the upper right corner of Fig. 2). The poles, corresponding with the reduced axial wavenumbers in the hard part of the duct, are given by

$$\gamma^{1-m}\,\mathrm{J}'_m(\Omega\gamma) = 0, \tag{23}$$

denoted by $\sigma = \sigma_{m\nu}$, implicitly given by $\Omega\gamma = \alpha_{m\nu}$, $\nu = 1, 2, \ldots$ where $\alpha_{m\nu}$ denote the non-trivial zeros of $\mathrm{J}'_m$. For hard-walled ducts, the left and right-running reduced wavenumbers are symmetric, and so the left-running hard-wall modes are given by $\sigma = -\sigma_{m\nu}$.

In the usual way [55] we split $K$ into functions that are analytic in the upper and in the lower half-plane (but note a possible instability pole in the upper half-plane that really is to be counted to the lower half-plane; see Eq. (28) and below)

$$K(\sigma) = \frac{K_+(\sigma)}{K_-(\sigma)}. \tag{24}$$

[4] One for each impedance surface, as follows from the surface wave arguments set out in [24] and the numerical examples te be given below.

Following Appendix A, we introduce the auxiliary split functions $N_+$ and $N_-$, satisfying

$$K(\sigma) = \frac{N_+(\sigma)}{N_-(\sigma)} \tag{25}$$

and given by

$$\log N_\pm(\sigma) = \frac{1}{2\pi \mathrm{i}} \int_0^\infty \left[ \frac{\log K(u)}{u-\sigma} - \frac{\log K(-u)}{u+\sigma} \right] \mathrm{d}u, \tag{26}$$

where the integration contours are near but not exactly along the real axis in the way as explained in Appendices A and B. The $+$ sign corresponds with $\Im\mathfrak{m}\ \sigma > 0$ or $\Im\mathfrak{m}\ \sigma = 0$ & $\Re\mathfrak{e}\ \sigma < 0$, and the $-$ sign with $\Im\mathfrak{m}\,\sigma < 0$ or $\Im\mathfrak{m}\ \sigma = 0$ & $\Re\mathfrak{e}\ \sigma > 0$. (Use for points from the opposite side the definition $K N_- = N_+$.) Following Appendix A, we obtain the following asymptotic behaviour

$$N_\pm(\sigma) = \mathcal{O}(\sigma^{\pm 1/2}). \tag{27}$$

When no instability pole crosses the contour, we identify

$$K_+(\sigma) = N_+(\sigma), \quad K_-(\sigma) = N_-(\sigma). \tag{28}$$

When an instability pole $\sigma_{HI}$ crosses the contour and is to be included among the right-running modes of the lower halfplane, $N_-$ contains the factor $(\sigma - \sigma_{HI})^{-1}$, so the causal split functions are

$$K_+(\sigma) = (\sigma - \sigma_{HI}) N_+(\sigma), \quad K_-(\sigma) = (\sigma - \sigma_{HI}) N_-(\sigma). \tag{29}$$

We continue with our analysis. We substitute the split functions in Eq. (20) to get

$$K_-(\sigma) P_-(\sigma) + \mathrm{i}\beta\, \mathrm{J}_m(\alpha_{m\mu}) \frac{K_-(\sigma) - K_-(\sigma_{m\mu})}{\Omega(\sigma - \sigma_{m\mu})} = -K_+(\sigma) H_+(\sigma) - \frac{\mathrm{i}\beta\, \mathrm{J}_m(\alpha_{m\mu}) K_-(\sigma_{m\mu})}{\Omega(\sigma - \sigma_{m\mu})}. \tag{30}$$

The left-hand side is a function that is analytic in the lower half-plane, while the right-hand side is analytic in the upper half-plane. So together they define an entire function $E$.

From the estimate $h(x) = \mathcal{O}(x^\eta)$ for $x \downarrow 0$ and $\eta > 0$, it follows [55, p. 36], that

$$H_+(\sigma) = \mathcal{O}(\sigma^{-\eta-1}) \quad (|\sigma| \to \infty, \Im\mathfrak{m}(\sigma) > 0). \tag{31}$$

This gives us the information to determine $E$. If there is no instability pole, then $K_+(\sigma) H_+(\sigma) = \mathcal{O}(\sigma^{-\eta-1/2})$, and so $E$ vanishes at infinity and has to vanish everywhere according to Liouville's theorem [55]. If there is an instability pole, we have an extra factor $\sigma$ and so $K_+(\sigma) H_+(\sigma) = \mathcal{O}(\sigma^{-\eta+1/2})$. This means that if $\eta = 1/2$ (no smooth streamline at $x = 0$, i.e., no Kutta condition), the entire function is only bounded and equal to a constant. If unmodelled physical effects (nonlinearities, viscosity) require a smooth behaviour of $h$ near $x = 0$, i.e., the Kutta condition, we have to choose $E = 0$, as this yields $\eta = 3/2$. This is illustrated schematically in Fig. 3.

We will start with the assumption of an instability pole. As we will see, the other case will be automatically included in the formulas, and it will not be necessary to consider both cases separately.

We scale the constant $E$,

$$E = \frac{-\mathrm{i}\beta\, \mathrm{J}_m(\alpha_{m\mu}) K_-(\sigma_{m\mu})}{\Omega(\sigma_{HI} - \sigma_{m\mu})}(1-\Gamma) = -\frac{\mathrm{i}\beta}{\Omega}\, \mathrm{J}_m(\alpha_{m\mu}) N_-(\sigma_{m\mu})(1-\Gamma), \tag{32}$$

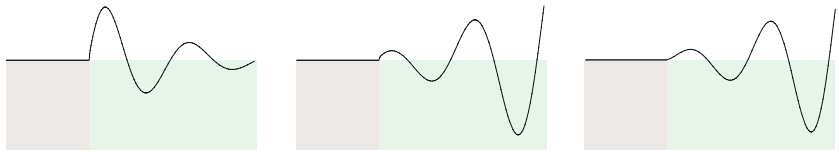


**Fig. 3** Types of edge singularity. Note that in the Ingard–Myers model the perturbed wall streamline does *not* cross the wall. It is positioned slightly off the wall at a distance small compared to a wavelength but large compared to any acoustic perturbation. (**a**) no Kutta condition, no instability, (**b**) no Kutta condition, instability, (**c**) Kutta condition, instability

such that $\Gamma = 0$ corresponds with no excitation of the instability (no contribution from $\sigma_{HI}$), while $\Gamma = 1$ corresponds with the full Kutta condition. Anything in between will correspond to a certain amount of instability wave, but not enough to produce a smooth solution in $x = 0$. It is readily verified that the assumption of *no* instability pole, i.e., $K_+ = N_+$ and $E = 0$, leads to exactly the same formula as with $\Gamma = 0$. So in the following we will identify with condition $\Gamma = 0$ both the situation of no instability pole and the situation of an instability that is (for whatever reason) not excited.

The total solution is now given by the following inverse Fourier integral, with a deformation around the pole $\sigma = \sigma_{HI}$ if $\Gamma \neq 0$:

$$p = p_{\text{in}} + \frac{\Omega}{2\pi \mathrm{i}\beta^2} \mathrm{J}_m(\alpha_{m\mu}) N_-(\sigma_{m\mu}) \int_{-\infty}^{\infty} \frac{(1-M\sigma)^2 \mathrm{J}_m(\Omega\gamma r)}{\gamma \mathrm{J}'_m(\Omega\gamma) N_+(\sigma)} \cdots \\ \times \left[ \frac{1}{\sigma - \sigma_{m\mu}} - \frac{\Gamma}{\sigma - \sigma_{HI}} \right] \exp\Big( \mathrm{i} \frac{\Omega}{\beta} (M - \sigma) x \Big) \, \mathrm{d}\sigma. \tag{33}$$

(Note that the latter deformation will result in a residue contribution if $x > 0$.) For $x < 0$ we close the contour around the lower complex half-plane, and sum over the residues of the poles in $\sigma = -\sigma_{m\nu}$, the axial wavenumbers of the left-running hard-walled modes. We obtain the field

$$p = p_{\text{in}} + \sum_{\nu=1}^{\infty} R_{m\mu\nu} \mathrm{J}_m(\alpha_{m\nu}) \exp\Big( \mathrm{i} \frac{\Omega}{\beta} (M + \sigma_{m\nu}) x \Big), \tag{34}$$

where

$$R_{m\mu\nu} = \frac{\mathrm{J}_m(\alpha_{m\mu}) N_-(\sigma_{m\mu}) (1 + M\sigma_{m\nu})^2}{\beta^2 \sigma_{m\nu} \Big( 1 - \dfrac{m^2}{\alpha_{m\nu}^2} \Big) \mathrm{J}_m(\alpha_{m\nu}) N_+(-\sigma_{m\nu})} \left[ \frac{1}{\sigma_{m\nu} + \sigma_{m\mu}} - \frac{\Gamma}{\sigma_{m\nu} + \sigma_{HI}} \right]. \tag{35}$$

In particular

$$R_{011} = \frac{1+M}{1-M} \frac{N_-(1)}{N_+(-1)} \left[ \frac{1}{2} - \frac{\Gamma}{1 + \sigma_{HI}} \right]. \tag{36}$$

For the transmitted field in $x > 0$ we close the contour around the upper half-plane and sum over the residues from $\sigma = \tau_{m\nu}, \sigma_{m\mu}$ and (if $\Gamma \neq 0$) $\sigma = \sigma_{HI}$. We note that the residue from $\sigma = \sigma_{m\mu}$ just cancels $p_{in}$, while the other residues (except from $\sigma_{HI}$) are found after employing the change of notation (cf. Eq. (22))

$$\gamma \mathrm{J}'_m(\Omega\gamma) N_+(\sigma) = \frac{\Omega}{\beta^2} \chi(\sigma) N_-(\sigma). \tag{37}$$

Hence, we obtain

$$p = \sum_{\nu=1}^{\infty} T_{m\mu\nu}\, \mathrm{J}_m(\beta_{m\nu} r) \exp\Big(\mathrm{i}\frac{\Omega}{\beta}(M-\tau_{m\nu})x\Big) \\ -\Gamma\frac{\Omega^2}{\beta^2}\, \mathrm{J}_m(\alpha_{m\mu}) N_-(\sigma_{m\mu}) \frac{(1-M\sigma_{HI})^2}{\beta_{HI}\, \mathrm{J}'_m(\beta_{HI}) N_+(\sigma_{HI})}\, \mathrm{J}_m(\beta_{HI} r) \exp\Big(\mathrm{i}\frac{\Omega}{\beta}(M-\sigma_{HI})x\Big), \tag{38}$$

where $\beta_{m\nu} = \Omega\gamma(\tau_{m\nu})$, $\beta_{HI} = \Omega\gamma(\sigma_{HI})$, and

$$T_{m\mu\nu} = -\frac{\beta\, \mathrm{J}_m(\alpha_{m\mu}) N_-(\sigma_{m\mu})(1-M\tau_{m\nu})^2}{\chi'(\tau_{m\nu}) N_-(\tau_{m\nu})} \left[\frac{1}{\tau_{m\nu}-\sigma_{m\mu}} - \frac{\Gamma}{\tau_{m\nu}-\sigma_{HI}}\right], \tag{39}$$

while $\chi'(\tau_{m\nu})$ can be further specified to be

$$\chi'(\tau_{m\nu}) = -\mathrm{i}\beta^2 Z\, \mathrm{J}_m(\beta_{m\nu}) \left[\omega\tau_{m\nu}\Big(1 - \frac{m^2}{\beta_{m\nu}^2} - \frac{\Lambda_{m\nu}^4}{(\omega\beta_{m\nu}Z)^2}\Big) - \frac{2\mathrm{i}M\Lambda_{m\nu}}{\omega Z}\right], \tag{40}$$

in which

$$\Lambda_{m\nu} = \frac{\omega(1-M\tau_{m\nu})}{\beta^2}. \tag{41}$$

## 5 Causality

### 5.1 The CL test

To determine the direction of propagation of the modes, and thus detect any possible instability, we have available the following causality criteria:

- The Briggs–Bers [26–28] formalism (BB), where analyticity in the whole lower complex $\omega$-plane is enforced by tracing the poles for fixed $\mathfrak{Re}(\omega)$, and $\mathfrak{Im}(\omega)$ running from 0 to $-\infty$.
- The Crighton–Leppington [29,30] formalism (CL), where analyticity in the whole lower complex $\omega$-plane is enforced by tracing the poles for fixed (but large enough) $|\omega|$, and $\arg(\omega)$ running from 0 to $-\frac{1}{2}\pi$.

The CL test was originally devised for a pure Helmholtz instability without other length scales involved than the acoustic wavelength. In this case it is sufficient to rotate $\omega$ to the imaginary axis. If the situation is more complex, involving other length scales, $\omega$ may have to be increased first.

Unfortunately, the BB criterion is not applicable to Helmholtz-type instabilities as it requires the system to have a maximum temporal growth rate for all real wavenumbers. With Helmholtz instabilities the growth rate is not bounded since the axial wavenumber is asymptotically linearly proportional to the frequency. So we will use the CL procedure, but supported by an analysis of the modes for a vortex sheet at a finite distance away from the impedance wall. This analysis will clearly show that the suspected instability is indeed the offspring of the genuine Helmholtz instability of the free vortex sheet.

For definiteness we will model the complex, frequency-dependent impedance as a simple mass-spring-damper system

$$Z(\omega) = R + \mathrm{i}a\omega - \frac{\mathrm{i}b}{\omega}, \tag{42}$$

which satisfies the fundamental requirements for $Z$ to be physical and passive (see e.g. [60]), viz. $Z$ is analytic and non-zero in $\mathfrak{Im}(\omega) < 0$, $Z(\omega) = Z^*(-\omega)$ and $\mathfrak{Re}(Z) > 0$.

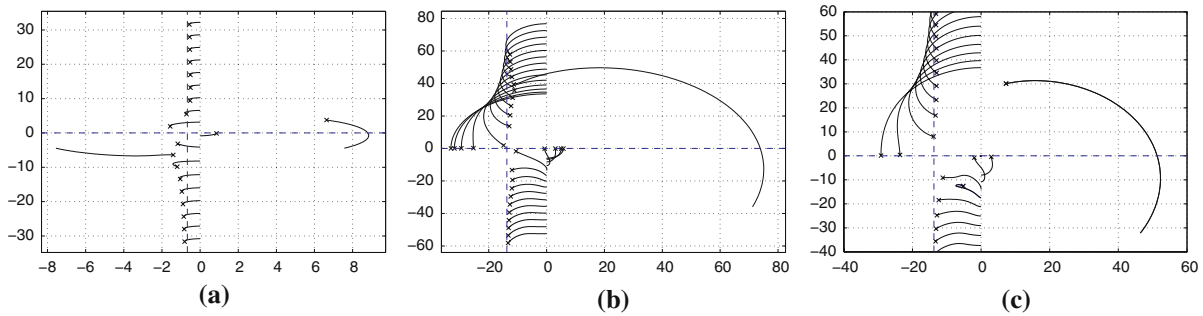


**Fig. 4** Causality contours for complex $\omega$ according to the Crighton–Leppington formalism. According to CL, the mode that changes from upper to lower half-plane is unstable. The crosses indicate the location of the modes when $\Im\mathrm{m}(\omega) = 0$. (**a**): $Z = 1 - 0.9\mathrm{i}$, $\omega = 1$, $M = 0.5$, $m = 0$, $a = 0.1$, $b = 1$ (**b**) $Z = 1 + 3.335\mathrm{i}$, $\omega = 10$, $M = 0.7$, $m = 0$, $a = 0.335$, $b = 0.15$ (**c**) $Z = 1 + 1.385\mathrm{i}$, $\omega = 10$, $M = 0.7$, $m = 5$, $a = 0.15$, $b = 1.15$

The analysis described in [29] concerns the causal solution for scattering of acoustic waves by a semi-infinite vortex sheet, and in many ways can therefore be thought of as being analogous to the problem considered in the present paper (see e.g. Sect. 5.2 ). Specifically, the difficulty associated with the unbounded growth rate of the vortex sheet is tackled in [29,30] by first supposing that the argument of $\omega$ is close to (with the present sign convention) $-\frac{1}{2}\pi$. This approach, which may be considered as a stronger version of Lighthill's argument of a slowly increasing source strength $\sim \mathrm{e}^{\mathrm{i}\omega t+\varepsilon t}$ in [16,17], yields a causal result, since the solution then decays to zero as $t \to -\infty$. Once the Fourier transform has been determined with imaginary $\omega$, the idea is then to attempt to analytically continue the Fourier transform back to the physically relevant case of real $\omega$. So we set

$$\omega = |\omega| \exp(\mathrm{i}\varphi), \tag{43}$$

and allow $\varphi$ to increase from $-\frac{1}{2}\pi$ to 0. As $\varphi$ increases, the singularities in the Fourier transform will move in the $\kappa$-plane, and to retain analyticity we must deform the $\kappa$ inversion contour so as to prevent any singularities crossing it. The singularities correspond to the $\kappa$ roots of (22), and their motion in typical cases is shown in Fig. 4. Note that in each case it is only the single surface wave which crosses the real $\kappa$-axis, having started in the lower half of the $\kappa$-plane when $\varphi = -\frac{1}{2}\pi$. It therefore follows that, in order to avoid a pole crossing, the $\kappa$ inversion contour must be deformed so as to run above this pole. This means that the surface wave is picked up when the spatial contour is closed in the lower half-plane for $x > 0$, and corresponds to a downstream instability. We can therefore conclude that in each of the cases described in Fig. 4 the Crighton–Leppington method predicts that the system is unstable.

This is not only typical of the cases we have considered—including various impedance models—but also in agreement with analytical results. For the special case of a semi-infinite 2D halfspace in the incompressible limit it was shown analytically in [24] that the system is unstable according to the Crighton–Leppington procedure.

In general, however, it appears that, in order to use this procedure to test the stability of our system, we need to solve the dispersion relation numerically, tracking the progress of the possible instability in the $\kappa$-plane as $\varphi$ is increased from $-\frac{1}{2}\pi$ to 0.

### 5.2 A finite boundary-layer model

Since the Ingard–Myers boundary condition embodies the vanishing boundary-layer limit of a vortex sheet at a small distance from the wall, we investigate here the behaviour of the modes in this limit in more detail (Fig. 5).

Consider the following (dimensionless) model for a finite boundary layer, consisting of a depth $\delta$ of stationary fluid underlying the flow:

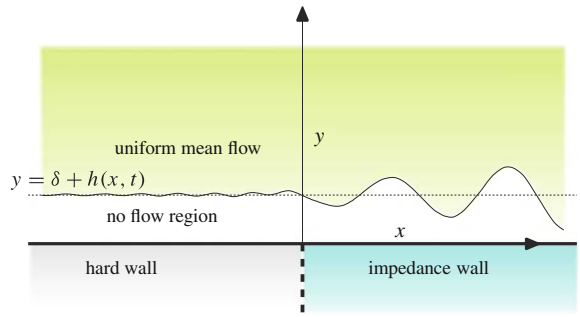


**Fig. 5** Sketch of finite boundary-layer model near the hard–soft transition point

$$0 < y < \delta : \nabla^2\phi + \omega^2\phi = 0, \qquad p = -\mathrm{i}\omega\phi, \tag{44}$$

$$\delta < y < \infty : \nabla^2\phi - \Big(\mathrm{i}\omega + M\frac{\partial}{\partial x}\Big)^2\phi = 0,\ p = -\Big(\mathrm{i}\omega + M\frac{\partial}{\partial x}\Big)\phi, \tag{45}$$

with boundary condition at $y = 0$

$$-Z\frac{\partial\phi}{\partial y} = p, \tag{46}$$

(which includes a hard wall with $Z \to \infty$) and continuity conditions across the vortex sheet at $y = \delta$

$$y \downarrow \delta : \frac{\partial\phi}{\partial y} = \Big(\mathrm{i}\omega + M\frac{\partial}{\partial x}\Big)h, \tag{47}$$

$$y \uparrow \delta : \frac{\partial\phi}{\partial y} = \mathrm{i}\omega h, \tag{48}$$

$$p\big|_{y\uparrow\delta} = p\big|_{y\downarrow\delta}. \tag{49}$$

For a stability analysis of the vortex sheet we look for solutions that decay for $y \to \infty$. Consider

$$\phi(x,y) = \mathrm{e}^{-\mathrm{i}\kappa x}\begin{cases} A\,\mathrm{e}^{-\mathrm{i}w(y-\delta)} + B\,\mathrm{e}^{-\mathrm{i}w(y-\delta)}, & 0 < y < \delta, \\ \mathrm{e}^{-\mathrm{i}v(y-\delta)}, & y > \delta, \end{cases} \tag{50}$$

where

$$v^2 = (\omega - \kappa M)^2 - \kappa^2, \quad w^2 = \omega^2 - \kappa^2,$$

with branches and branch cuts chosen such that $\Im\mathrm{m}(v) \leqslant 0$, $\Im\mathrm{m}(w) \leqslant 0$ and $w(0) = v(0) = \omega$. From the boundary and continuity conditions it follows that

$$A = \frac{(\omega - \kappa M)^2 w + \omega^2 v}{2\omega(\omega - \kappa M)w}, \quad B = \frac{(\omega - \kappa M)^2 w - \omega^2 v}{2\omega(\omega - \kappa M)w},$$

while the axial wavenumbers $\kappa$ are given by the eigenvalue equation

$$\frac{(\omega - \kappa M)^2 + \omega v Z}{(\omega - \kappa M)^2 w^2 Z + \omega^3 v} = -\mathrm{i}\frac{\tan(w\delta)}{w\omega} \tag{51}$$

For $\omega\delta \to \infty$, $\tan(w\delta) \to -\mathrm{i}$, we obtain

$$\big((\omega - \kappa M)^2 w + \omega^2 v\big)\big(\omega + wZ\big) = 0 \tag{52}$$

with two or four solutions, depending on the sign of $\mathfrak{Im}(Z)$. If $\mathfrak{Im}(Z) < 0$, acoustic surface waves of the impedance wall are possible, given by [24]

$$\kappa_S^{\pm} = \pm\omega\sqrt{1 - Z^{-2}}. \tag{53}$$

For the other cases, with $\mathfrak{Im}(Z) \geqslant 0$, no wall surface waves are possible. In either case the vortex sheet carries hydrodynamic waves, given by Miles [61]

$$\kappa_H^{\pm} = \frac{\omega}{2M}\Big(1 + \sqrt{1 + M^2} \pm \mathrm{i}\sqrt{2 - M^2 + 2\sqrt{1 + M^2}}\Big). \tag{54}$$

These waves are known to propagate in the direction of the mean flow (see below), so with $M > 0$ they propagate to the right, with $\kappa_H^-$ exponentially decaying and $\kappa_H^+$ exponentially increasing. This increasing wave is known as the compressible Kelvin–Helmholtz instability [62,63].

Note that $\kappa_H^{\pm}$ are linearly dependent on $\omega$. The other modes $\kappa_S^{\pm}$ are not necessarily so, but they are linearly dependent for large and small $\omega$ if $Z(\omega)$ tends to infinity in these cases, which is plausible in any physical realisation.

Apart from the hydrodynamic instabilities of the type of $\kappa_H^{\pm}$ and acoustic surface waves of the type $\kappa_S^{\pm}$, there are also acoustic modes related to the duct between the wall and the vortex sheet. These are given asymptotically by

$$\kappa_n^{\pm} = \pm\Big(\frac{\mathrm{i}n\pi}{\delta} - \frac{\omega}{\pi n}\Big(\frac{\mathrm{i}\omega\delta}{2} + \frac{1}{Z}\Big)\Big) + \mathcal{O}(1/n^2) \tag{55}$$

for large $n$. For hard walls the equation reduces to

$$\omega^2 v + \mathrm{i}(\omega - \kappa M)^2 w \tan(w\delta) = 0 \tag{56}$$

which yields for $\delta = 0$ only $v(\kappa) = 0$ or $\kappa = \pm\omega$, which are not acceptable solutions. These are not waves that decay for $y \to \infty$, so will not exist without external excitation.

For a vortex sheet close to the soft wall, i.e., $\omega\delta \to 0$, we find to leading order

$$(\omega - \kappa M)^2 + \omega v Z = 0. \tag{57}$$

This equation has been studied extensively elsewhere [24,58]. It describes the mode that interests us here for the limit $\delta = 0$, i.e., with the Ingard–Myers condition. In fact, this equation allows 0, 1, 2, 3, or 4 solutions, depending on $Z$ and $M$. These (at most) four solutions are just descendants of the four $\kappa_H^{\pm}$ and $\kappa_S^{\pm}$ roots that exist for large $\delta$ (although not necessarily continuously connected by parameter $\delta$).

The other modes that exists for any nonzero $\delta$ are given asymptotically, for small $\omega\delta$, as

$$\kappa_n^{\pm} = \pm\Big(\frac{\mathrm{i}n\pi}{\delta} - \frac{\omega}{\pi n Z}\Big) + \mathcal{O}(\omega^2\delta). \tag{58}$$

For impedance $1 - 2\mathrm{i}$, chosen such that all surface waves continue to exist for all $\delta$, the typical location of the wavenumbers are given in Fig. 6. In Fig. 7 the wavenumbers of the same configurations are traced as functions of $\omega$ according to the CL test, with the impedance chosen as $Z = 1 - \mathrm{i}/\omega$. The other relations that were tested give very similar behaviour. Hydrodynamic surface wave $\kappa_H^+$ in the first quadrant, viz. what is known to be Helmholtz unstable for $\delta = \infty$, is clearly seen to be the mode that crosses the real axis into the fourth quadrant for *any* $\delta$, and therefore always corresponds to an instability. All others remain in the half-plane in which they started.

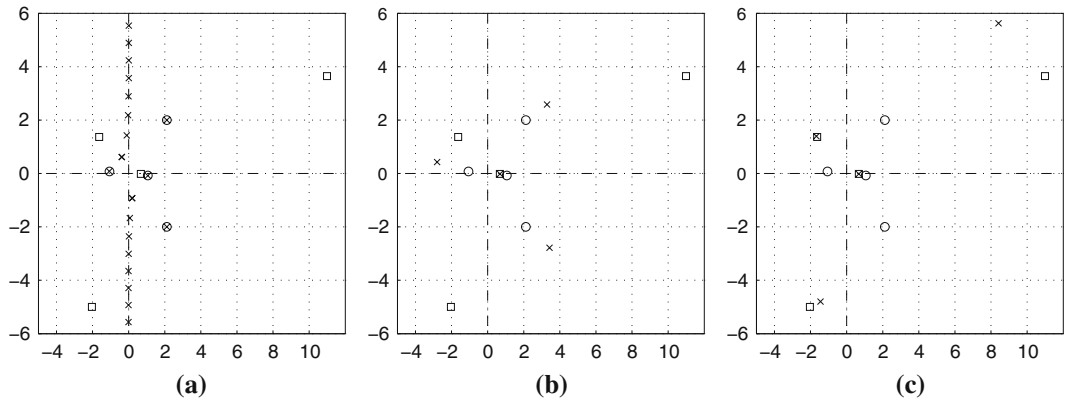


**Fig. 6** Typical location of axial mode numbers $\times$ for varying $\delta$, $\omega = 1$, $M = 0.5$, $Z = 1 - 2\mathrm{i}$. The four hydrodynamic and acoustic surface waves for $\delta = 0$ and $\delta = \infty$ are indicated by $\circ$ ($\delta = \infty$) and $\square$ ($\delta = 0$). (**a**) $\delta = 5$ (**b**) $\delta = 0.1$ (**c**) $\delta = 2 \cdot 10^{-3}$

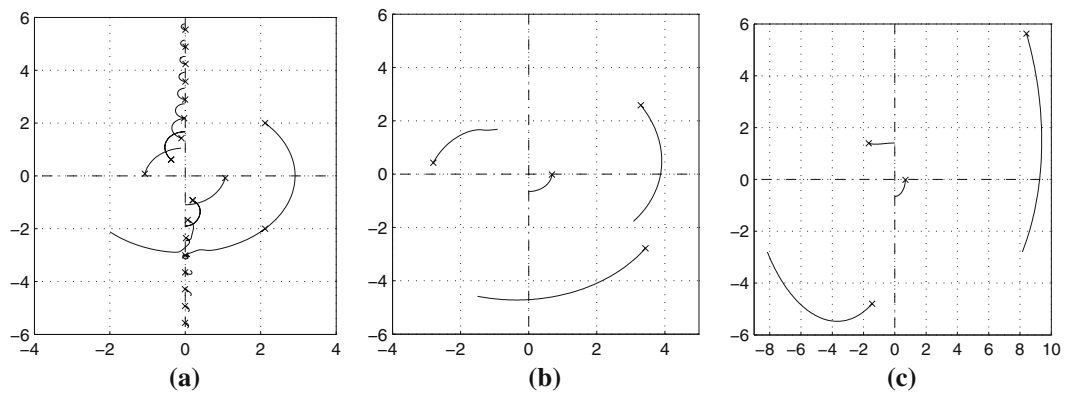


**Fig. 7** The axial wavenumbers are tracked for complex frequency $\omega = |\omega| \, \mathrm{e}^{\mathrm{i}\varphi}$ while $\varphi$ is varied from 0 to $-\pi/2$. According to the Crighton–Leppington formalism, a wavenumber that crosses from the upper half-plane to the lower half-plane corresponds to a right-running unstable mode. This is indeed in all cases the hydrodynamic wave in the first quadrant. While $Z(\omega) = 1 - \mathrm{i}/\omega$, all parameters are the same as in Fig. 6. (**a**) $\delta = 5$ (**b**) $\delta = 0.1$ (**c**) $\delta = 2 \cdot 10^{-3}$

### 5.3 Summary

In summary, we can conclude that our model system is genuinely unstable for the situations described in Fig. 4 where the vortex sheet is positioned at the wall, as well as for the related models of a vortex sheet at a finite distance from the wall where the stability properties of the system simplify to that of the well-established Kelvin–Helmholtz instability. Indeed, this has hardly been questioned since it has recently been confirmed numerically by Chevaugeon et al. [64].

It should of course be noted that this conclusion is to some extent dependent on the functional relationship between $Z$ and $\omega$. Different impedance models may call for further study, especially when the wall is lined by other than locally reacting material.

The above conclusion relates to the present model. An entirely different question is whether the physical reality is unstable. It will certainly not be unstable to the extent of streamline deflections of the order of the boundary-layer thickness; that would be prevented by the impenetrable wall. However, nothing is yet known about what might happen at the very early stage.

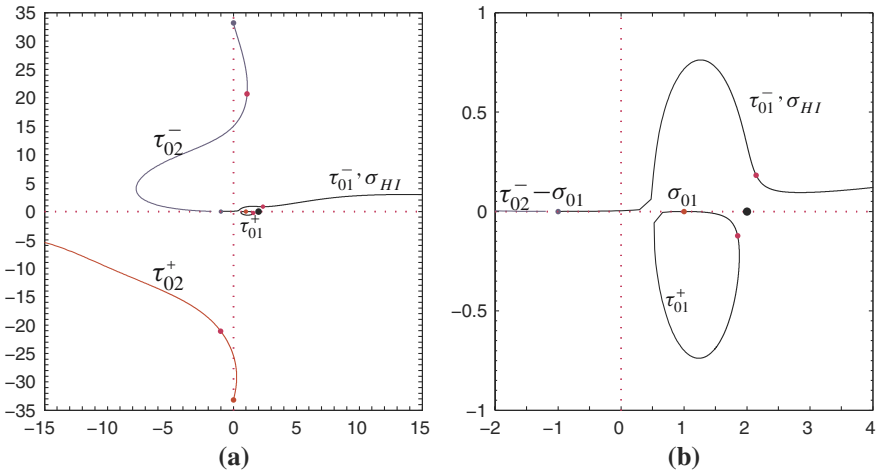


**Fig. 8** Modal wavenumbers $\tau_{0\nu}^{\pm}$ as they traverse the complex $\sigma$-plane for varying impedance $Z = 1 + \mathrm{i}\lambda$. (**a**) $\omega = 0.1, \Re\mathfrak{e}(Z) = 1, m = 0, M = 0.5$ (**b**) $\omega = 0.01, \Re\mathfrak{e}(Z) = 1, m = 0, M = 0.5$

## 6 Low-frequency asymptotics

An interesting limit in the present context is the one for small $\omega$. In this case the transmitted wave is very small and the reflection coefficient $R_{011}$ of the plane wave is of main interest. We have for small $\omega$, from (21),

$$K(\sigma) = -2\frac{(1 - M\sigma)^2}{\beta^2\gamma(\sigma)^2} + \mathcal{O}(\omega) \quad (\omega \to 0). \tag{59}$$

The double zeros $\sigma = M^{-1}$ arise from two modes, one from the upper half-plane and one from the lower half-plane that meet each other at $\omega = 0$. These modes are of surface-wave type [24] because the radial wavenumber is purely imaginary, but for low $\omega$ the radial decay is so slow that their confinement to the wall inside the duct is meaningless. The mode from the upper half-plane is (in all cases considered) the instability $\sigma_{HI}$. The other one is, in the nomenclature of [24], the right-running acoustic surface wave $\sigma_{SR}$. In the present notation it is a mode from the set $\{\tau_{0\nu}\}$, say,[5] $\tau_{01}$ or (to avoid any ambiguity) $\tau_{01}^+$. For small but non-zero $\omega$ they are asymptotically given by

$$\sigma_{HI} = M^{-1} + \frac{1}{2}(1 + \mathrm{i})\beta^2 M^{-2}\sqrt{\omega Z} + \cdots, \tag{60a}$$

$$\tau_{01}^+ = M^{-1} - \frac{1}{2}(1 + \mathrm{i})\beta^2 M^{-2}\sqrt{\omega Z} + \cdots. \tag{60b}$$

This is illustrated by Fig. 8. The first two left- and right-running modes are drawn as a function of $Z = 1 + \mathrm{i}\lambda$, where $\lambda$ is varied from $\infty$ (hard wall) to $-\infty$ (again hard wall). Starting as the right-running hard-wall plane wave $\sigma_{01} = 1$, $\tau_{01}^+$ becomes slightly complex, resides near $M^{-1}$ when $\lambda = 0$, but returns to its starting hard-wall value when $\lambda \to -\infty$. The second right-running mode $\tau_{02}^+$ (the first cut-off) disappears to real $-\infty$. The left-running mode $\tau_{01}^-$ starts as the hard-wall plane-wave mode $-\sigma_{01} = -1$, then moves to the right, resides near $M^{-1}$ when $\lambda = 0$ (where it apparently has changed its character and has become a *right*-running instability wave !) and then, instead of returning to its original hard-wall value, it disappears to real $+\infty$. Its position has been taken over by the second left-running mode $\tau_{02}^-$.

[5] There is no obvious way of sorting soft-wall modes; see Fig. 8.

Now we can approximate the split functions

$$N_+(\sigma) \simeq -2\frac{1-M\sigma}{\beta^2(1-\sigma)}, \quad N_-(\sigma) \simeq \frac{1+\sigma}{1-M\sigma}, \tag{61}$$

not necessarily with the same multiplicative factor as would arise from representation (A.9). For the plane-wave reflection coefficient this yields

$$R_{011} \simeq -\frac{1+M}{1-M}\Big(1-\frac{2M\Gamma}{1+M}\Big)+\cdots \quad (\omega \to 0), \tag{62}$$

resulting in the remarkably different values $R_{011} = -1$ for $\Gamma = 1$ and $R_{011} = -(1+M)/(1-M)$ for $\Gamma = 0$, irrespective of $Z$ (although the limit $Z \to \infty$, $\omega \to 0$ will be non-uniform). This result is exactly the same as found for the low-frequency plane-wave reflection coefficients of a semi-infinite duct with jet or uniform mean flow [40,45–48].

The instability wave corresponding to (60a), with axial wavenumber equal to the Strouhal number $\omega/M$, vanishes in pressure, due to the factor $(1-M\sigma_{HI})$, but survives in the potential or velocity. The transmission coefficient of the wave corresponding to (60b), with the same axial wavenumber, appears to be

$$T_{011} \simeq \frac{1}{2}\Gamma\Big(\frac{1+M}{1-M}\Big)^{1/2}+\cdots. \tag{63}$$

## 7 Results

In order to illustrate the above results we have evaluated numerically (see Appendix) the reflection coefficients $R_{011}$ of the right-running plane-wave mode (with $m = 0$ and $\mu = 1$) into the left-running plane wave (also with $\mu = 1$) as a function of frequency $\omega$, and reflection coefficient $R_{111}$ of the right-running $m\mu = 11$-mode into its left-running $m\mu = 11$-counterpart. The impedance $Z = 1 - 2\mathrm{i}$ and the Mach number $M = 0.5$ are chosen as typical of an aero-engine inlet lining, but are otherwise not special. Both modulus $|R_{.11}|$ and phase $\phi_{.11}$ are plotted, but for the lower frequencies the plane-wave phase is reformulated to an end correction $\delta_{011}$, i.e., the virtual point beyond $x = 0$, scaled by $\omega$, where the wave seems to reflect with condition $|p|$ being minimal. Since

$$\Big|\mathrm{e}^{-\mathrm{i}\frac{\omega}{1+M}x}+R_{011}\,\mathrm{e}^{\mathrm{i}\frac{\omega}{1-M}x}\Big|^2 = 1+|R_{011}|^2+2|R_{011}|\cos\Big(\tfrac{2\omega}{1-M^2}x+\phi_{011}\Big)$$

is minimal if $\frac{2\omega}{1-M^2}x+\phi_{011} = \pi$, so

$$\delta_{011} = (1-M^2)\frac{\pi-\phi_{011}}{2\omega}. \tag{64}$$

In order to facilitate comparison with the low-$\omega$ analysis, the results are given, both for a small interval $0 \leqslant \omega \leqslant 1$ and a large interval $0 \leqslant \omega \leqslant 15$. (The end-correction is given only for the small interval because it loses its meaning for higher frequencies.) The most striking result is probably the confirmation of the analytically determined reflection coefficients 1 ($\Gamma = 1$, Fig. 9 left) and $(1+M)/(1-M)$ ($\Gamma = 0$, Fig. 10 left) for $\omega \to 0$, and in addition that the end correction tends to a finite value (Kutta condition; Fig. 9 right) and to $\infty$ (no Kutta condition; Fig. 10 right). All this is in exact analogy with the reflection of low-frequency sound waves at the exit plane of a free jet [47] (Figs. 11, 12). Note that this behaviour is not related to $\omega = 0$, being a resonance frequency because $R_{111}$ tends to 1 at its first resonance frequency in both cases (Figs. 13 and 14).

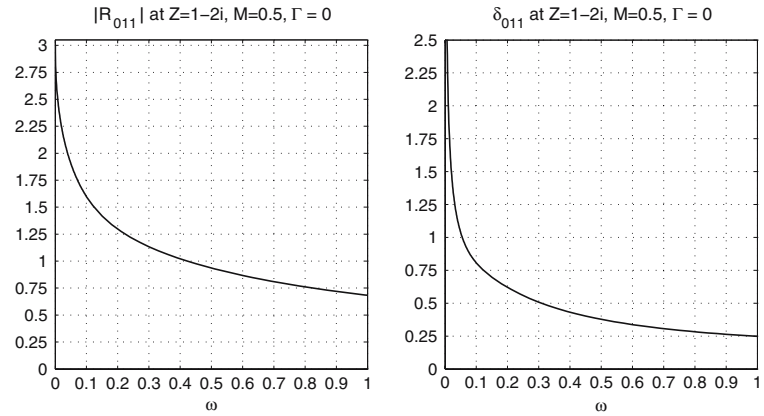


**Fig. 9** Modulus of reflection coefficient and end correction for right-running plane wave ($m\mu = 01$) into left-running plane wave, where the plane wave is incident from hard-walled section to lined section with impedance $Z = 1 - 2\mathrm{i}$, while $M = 0.5$. Without Kutta condition at $x = 0$

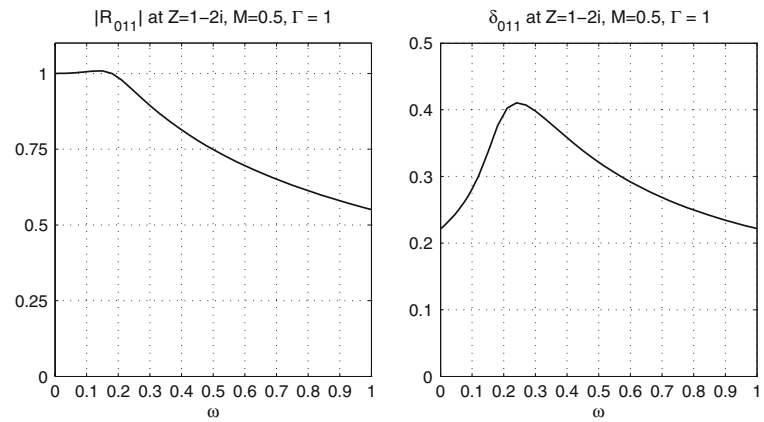


**Fig. 10** Modulus of reflection coefficient and end correction for right-running plane wave ($m\mu = 01$) into left-running plane wave, where the plane wave is incident from hard-walled section to lined section with impedance $Z = 1 - 2\mathrm{i}$, while $M = 0.5$. With Kutta condition at $x = 0$

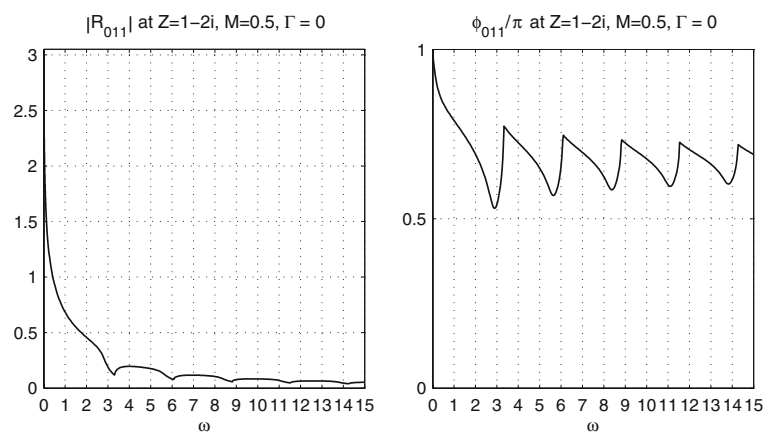


**Fig. 11** Modulus and phase of reflection coefficient for right-running plane wave ($m\mu = 01$) into left-running plane wave. Same conditions as Fig. 9 but with larger frequency range

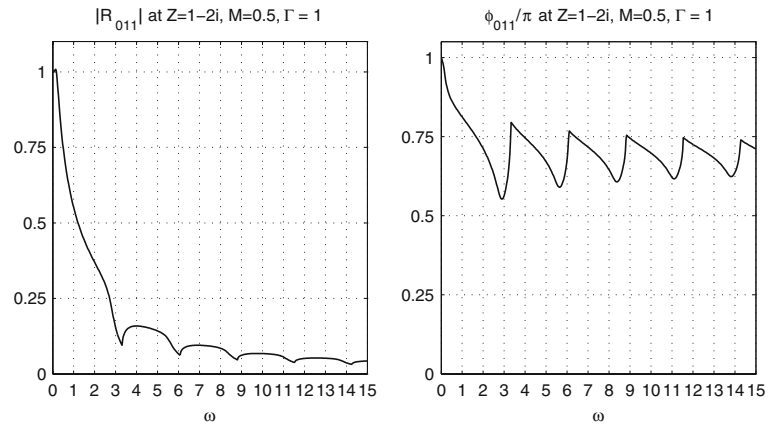


**Fig. 12** Modulus and phase of reflection coefficient for right-running plane wave ($m\mu = 01$) into left-running plane wave. Same conditions as Fig. 10 but with larger frequency range

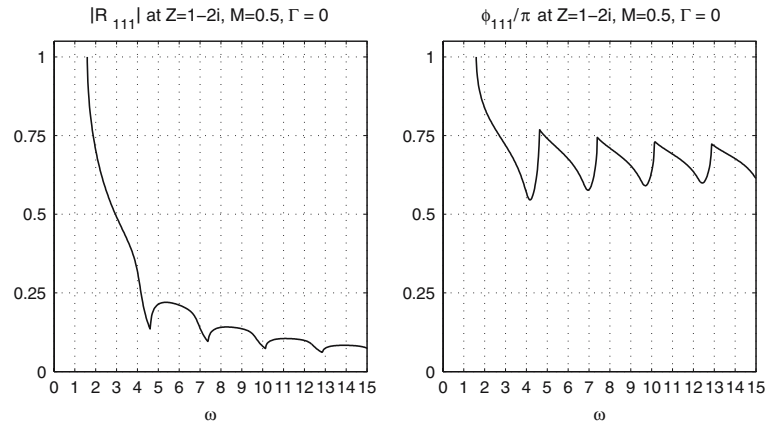


**Fig. 13** Modulus and phase of reflection coefficient for right-running $m\mu = 11$-mode into the same left-running mode. Otherwise same conditions as in Fig. 11

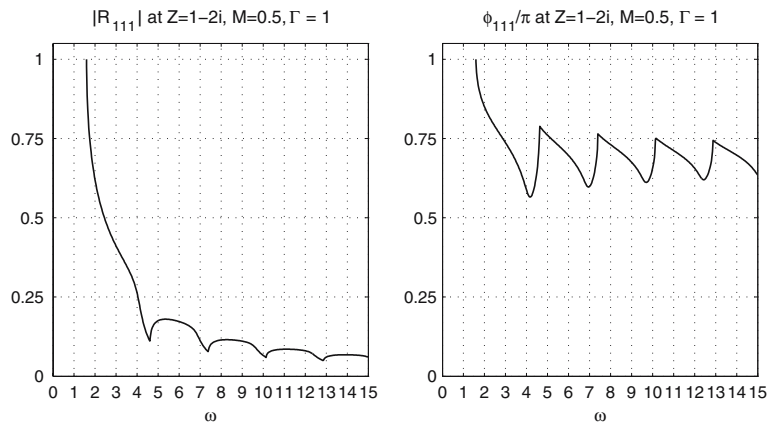


**Fig. 14** Modulus and phase of reflection coefficient for right-running $m\mu = 11$-mode into the same left-running mode. Otherwise same conditions as in Fig. 12

## 8 Conclusions

An explicit Wiener–Hopf solution has been derived to describe the scattering of duct modes at a hard–soft wall impedance transition at $x = 0$ in a circular duct with uniform mean flow. A mode, incident from the hard-walled upstream region, is scattered into reflected hard-wall and transmitted soft-wall modes. A plausible edge condition at $x = 0$ requires at least a continuous wall streamline $r = 1 + h(x, t)$, no more singular than $h = \mathcal{O}(x^{1/2})$ for $x \downarrow 0$. By analogy with a trailing-edge scattering problem, the possibility of vortex shedding from the hard–soft transition would allow us to apply the Kutta condition and require the edge condition to be no more singular than corresponding to $h = \mathcal{O}(x^{3/2})$ for $x \downarrow 0$.

The physical relevance of this Kutta condition is still an open question. It all depends on the direction of propagation of the soft-wall modes. The Wiener–Hopf analysis shows that no Kutta condition can be applied if none of the apparently upstream running, decaying, soft-wall modes is in reality a downstream-running instability. However, causality analyses in the complex frequency domain, taking into account the frequency dependence of the impedance, indicate that, under certain circumstances, one soft-wall mode (per circumferential order) is to be considered as an instability. In this case we may be able to enforce a Kutta condition and thus excite the instability.

As the growth rate of this presumed instability may be very high, it remains to be seen if this result is an artefact of the linearised model or actually representative of reality. There is thus a need for clarifying and distinguishing experiments to be carried out. The available experiments [37,38] give indirect but convincing arguments for the possible existence of instability waves along the liner. It is, however, not clear yet what the contributions are of the liner's leading and trailing edge (the instability may interact with both), while the existence of the wave per se does not conclusively tell us what type of singularity to adopt in our model. Furthermore, the role of the boundary layer thickness (i.e., the Strouhal number based on the momentum thickness) is known to be important for the free shear layer [53] and may be relevant here too.

We have presented results for cases with Kutta and no Kutta condition applied, and showed that the difference is, for certain choices of parameters, large enough for experimental verification. In particular, for low Helmholtz numbers, the reflection properties become very simple and imitate the behaviour of the free jet. The pressure reflection coefficient for the plane wave in the low-Helmholtz-number regime is near unity with a Kutta condition, and near $(1 + M)/(1 - M)$ with no Kutta condition applied. This low-frequency limit has the advantage that the instability growth rate reduces to zero such that nonlinear effects of the instability are postponed, while the reflection coefficient becomes independent of the impedance. On the other hand, there is the practical disadvantage to be overcome that in any experimental set-up the lined section must be very long.

## Appendix A: Split functions

The complex function $K(\sigma)$ has poles and zeros in the complex plane, in particular also along the real axis. We need to evaluate $K$, written as a quotient of two functions that are respectively analytic in the upper and lower half-plane, and along the real $\kappa$-axis. For reasons of causality we need to start the analysis with a complex-valued $\omega$ (with $\Im\mathrm{m}(\omega) < 0$); see Sect. 5. In that case the zeros and poles and the real $\kappa$-axis, mapped (see (13)) into the $\sigma$-plane, are typically shifted into the complex plane as indicated in Fig. 15 (the $\kappa$-axis really rotates around $\sigma = M$ instead of 0, but as long as we remain in the region of analyticity we can shift the contour to the right). A set of split functions can now be constructed as follows. We want to write $K(\sigma)$ as the quotient of a function $K_+(\sigma)$, which is analytic and non-zero in the upper half-plane, and a function $K_-(\sigma)$ which is analytic and non-zero in the lower half-plane, while both are at most of algebraic growth at infinity:

$$K(\sigma) = \frac{K_+(\sigma)}{K_-(\sigma)}. \tag{A.1}$$

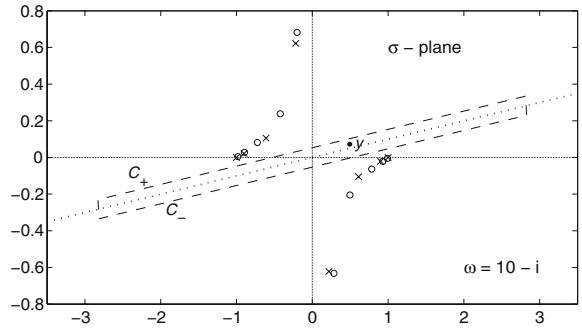


**Fig. 15** Sketch of zeros and poles of $K(\sigma)$ and contour of integration in the complex $\sigma$-plane for complex $\omega$

Construct an elongated rectangle $\mathcal{C} = \mathcal{C}_+ \cup \mathcal{C}_-$ along the rotated $\kappa$-axis, which for $\Im\mathrm{m}(\omega) < 0$ makes an angle with the real axis. Select a point $y$ inside $\mathcal{C}$. With $\mathcal{C}$ passing in positive orientation we have

$$\log K(y) = \frac{1}{2\pi \mathrm{i}} \oint_C \frac{\log K(u)}{u - y}\, \mathrm{d}u. \tag{A.2}$$

Let the ends of $C$ tend to $\pm\infty$ symmetrically. Since

$$\begin{aligned} K(\sigma) &\sim \tfrac{\Omega M^2}{\beta^2}\sigma - \tfrac{2M\Omega}{\beta^2} - \mathrm{i}\beta\Omega Z \ \ (\sigma \to \infty), \\ K(\sigma) &\sim -\tfrac{\Omega M^2}{\beta^2}\sigma + \tfrac{2M\Omega}{\beta^2} - \mathrm{i}\beta\Omega Z \ \ (\sigma \to -\infty), \end{aligned} \tag{A.3}$$

the contributions from the ends cancel each other to leading order, such that the total contribution tends to 0. In particular

$$\lim_{L\to\infty} \int_{-L}^{L} \frac{\log K(u)}{u - y}\, \mathrm{d}u = \lim_{L\to\infty} \int_0^L \frac{\log K(u)}{u - y} - \frac{\log K(-u)}{u + y}\, \mathrm{d}u = \int_0^\infty \left[\frac{\log K(u)}{u - y} - \frac{\log K(-u)}{u + y}\right] \mathrm{d}u \tag{A.4}$$

because

$$\frac{\log K(u)}{u - y} - \frac{\log K(-u)}{u + y} = \frac{2y}{u^2} \log\left(\frac{\Omega M^2}{\beta^2}\right) + \cdots \tag{A.5}$$

converges. Thus we can write

$$\log K(y) = \frac{1}{2\pi \mathrm{i}} \int_{C_-} \frac{\log K(u)}{u - y}\, \mathrm{d}u - \frac{1}{2\pi \mathrm{i}} \int_{C_+} \frac{\log K(u)}{u - y}\, \mathrm{d}u. \tag{A.6}$$

We can identify, respectively, $\log(K_+)$ and $\log(K_-)$ with the first and second integral to get

$$K_+(y) = \exp\Big[\frac{1}{2\pi \mathrm{i}} \int_{C_-} \frac{\log K(u)}{u - y}\, \mathrm{d}u\Big], \qquad K_-(y) = \exp\Big[\frac{1}{2\pi \mathrm{i}} \int_{C_+} \frac{\log K(u)}{u - y}\, \mathrm{d}u\Big], \tag{A.7}$$

because the respective domains can be extended in an upward and downward direction without passing any singularities (i.e., the integration contour). If we let $\Im\mathrm{m}(\omega) \uparrow 0$, we obtain the sought split functions $K_\pm$ for real $\omega$, provided we allow for any possible contour deformation if an instability pole crosses the real axis (see Sect. 5). It is, however, more convenient not to retain this deformed contour but write

$$K(\sigma) = \frac{N_+(\sigma)}{N_-(\sigma)}, \tag{A.8}$$

where both $N_+$ and $N_-$ are now always given by the expression

$$\log N_\pm(\sigma) = \frac{1}{2\pi \mathrm{i}} \int_0^\infty \left[ \frac{\log K(u)}{u-\sigma} - \frac{\log K(-u)}{u+\sigma} \right] \mathrm{d}u. \tag{A.9}$$

Wherever $\log K(u)$ is singular along the real axis, the integration contour is indented into the upper (in view of the limit $\mathfrak{Im}(\omega) \uparrow 0$ that is taken) complex plane (see also Appendix B). The $+$ sign corresponds with $\mathfrak{Im}\,\sigma > 0$ and $\mathfrak{Im}\,\sigma = 0$ and $\mathfrak{Re}\,\sigma < 0$, and the $-$ sign with $\mathfrak{Im}\,\sigma < 0$ or $\mathfrak{Im}\,\sigma = 0$ and $\mathfrak{Re}\,\sigma > 0$. (Use for points from the opposite side the definition $KN_- = N_+$.) As the split functions are defined up to a multiplicative constant that is determined by the method of calculation, it is instructive to note that constants, like $K(\sigma) = c$, and simple products, like $K(\sigma) = (\sigma - c_+)(\sigma - c_-)$, are split by (A.9) as follows.

$$c = \frac{c^{1/2}}{c^{-1/2}}, \quad (\sigma - c_+)(\sigma - c_-) = \frac{-\mathrm{i}(\sigma - c_-)}{-\mathrm{i}(\sigma - c_+)^{-1}} \quad (\mathfrak{Im}(c_\pm) \gtrless 0). \tag{A.10}$$

When no instability pole crosses the contour, we identify

$$K_+(\sigma) = N_+(\sigma), \quad K_-(\sigma) = N_-(\sigma). \tag{A.11}$$

When an instability pole $\sigma_{HI}$ crosses the contour, and is to be included among the right-running modes of the lower half-plane, we write

$$K_+(\sigma) = (\sigma - \sigma_{HI})N_+(\sigma), \quad K_-(\sigma) = (\sigma - \sigma_{HI})N_-(\sigma). \tag{A.12}$$

If we express

$$K(\sigma) = \mathrm{i}\Omega M^2 \beta^{-2} \gamma(\sigma) L(\sigma), \tag{A.13}$$

then $L$ is a well-behaved function, satisfying $L(\sigma) \to 1$ both for $\sigma \to \infty$ and $-\infty$, and can be split by the present method into functions that remain bounded (see [55, p.15, Theorem C]). The factor $\gamma(\sigma)$ can be split by inspection into the quotient of $(1-\sigma)^{1/2}$ and $(1+\sigma)^{-1/2}$. As a result, we have the asymptotic estimates

$$N_+(\sigma) = \mathcal{O}(\sigma^{1/2}), \quad N_-(\sigma) = \mathcal{O}(\sigma^{-1/2}) \quad \text{for } \sigma \to \pm\infty, \tag{A.14}$$

leading to corresponding behaviour for $K_+$ and $K_-$, depending on the included instability pole.

## Appendix B: Numerical evaluation of $K_\pm$

For numerical evaluation of the split functions, we need to evaluate the integral (A.9). First, we have to deal with any possible zeros and poles along the real axis. A natural way to avoid them is by deforming the contour into the upper complex plane, but taking good care to avoid any crossing of other poles or zeros (cf. [48]). A suitable choice was found to be given by the parameterisation $u = \xi(t)$ where

$$\xi(t) = t + \mathrm{i}d\frac{4t/q}{3 + (t/q)^4}, \quad 0 \leqslant t < \infty. \tag{B.15}$$

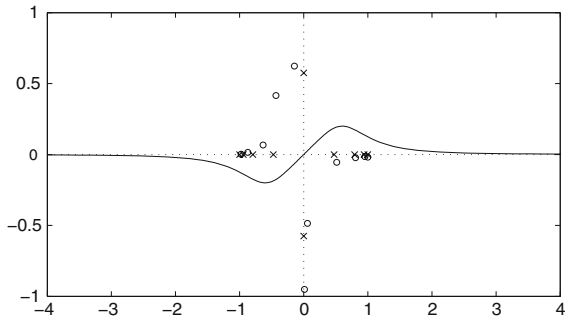

**Fig. 16** Deformed integration contour given by Eq. (B.15). Both $u = \xi(t)$ and $u = -\xi(t)$ are drawn ($Z = 2 - \mathrm{i}$, $\omega = 10$, $M = 0.5$, $m = 0$, $d = 0.2$, $q = 0.6$)

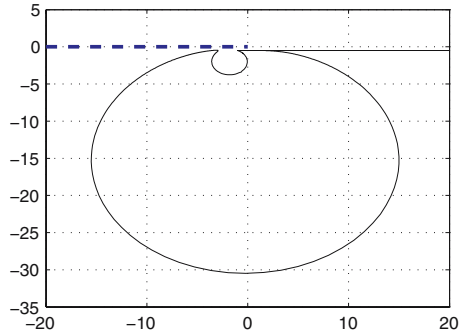

**Fig. 17** Tracing $K(u)$ in the complex plane when $u$ varies along the contour. Note that it never crosses the negative real axis, and indeed $K(u) \sim |u|$ for large $|u|$. $Z = 1 - 2\mathrm{i}$, $M = 0.5$, $\omega = 0.5$, $m = 0$, $d = 0.1$, $q = 1$

$q + \mathrm{i}d$ denotes the position of the top of the indentation (see Fig. 16), where $d$ and $q$ are adjustable constants that have to be chosen such that $q$ is large enough to avoid the real wavenumbers (usually between 0.5 and 1), while $d$ is positive but not too large in order to avoid enclosing possible surface waves in the first and third quadrant. This was tested in all cases considered by visual inspection. For example for very small $Z$ (see [24]), and for $m = 0$ and very small $\omega$, there is a surface wave that approaches the real value $\sigma = M^{-1}$ from above. The next step is to change the infinite integral into a finite integral by the transformation $t = \zeta(s)$ where

$$\zeta(s) = \frac{s}{(1-s)^2}, \quad 0 \leqslant s \leqslant 1. \tag{B.16}$$

This particular choice ensures that the resulting integral is easily evaluated by standard routines because the limiting value of the integrand at $s = 1$ is just zero. This is seen as follows. After both transformations we have

$$\int_0^\infty \left[\frac{\log K(u)}{u-\sigma} - \frac{\log K(-u)}{u+\sigma}\right] \mathrm{d}u = \int_0^1 \left[\frac{\log K(\xi(\zeta(s)))}{\xi(\zeta(s))-\sigma} - \frac{\log K(-\xi(\zeta(s)))}{\xi(\zeta(s))+\sigma}\right] \xi'(\zeta(s))\zeta'(s)\,\mathrm{d}s. \tag{B.17}$$

For $s \uparrow 1$, i.e., $u \to \infty$, we have

$$\left[\frac{\log K(\xi(\zeta(s)))}{\xi(\zeta(s))-\sigma} - \frac{\log K(-\xi(\zeta(s)))}{\xi(\zeta(s))+\sigma}\right] \xi'(\zeta(s))\zeta'(s) = 4\sigma \log\left(\frac{\Omega M^2}{\beta^2}\right)(1-s) + \cdots \to 0. \tag{B.18}$$

Finally, we mention the following very important condition for a correct split integral. It should always be checked if, anywhere along the contour, $K(u)$ crosses the branch cut of the logarithmic function, which is normally chosen along the negative real axis. Here, the integrand is not analytic, and if $K$ crosses the cut, the split integral would be invalid. An example of the behaviour of $K(u)$ is shown in Fig. 17.

**Acknowledgements** The present research started when the author visited the University of Cambridge under a grant of the Royal Society. The financial support is greatly acknowledged. The advice, discussions and interest of Nigel Peake and Ed Brambley were absolutely crucial, especially for the causality issue in an earlier version of the paper.

## References

1. Crighton DG, Pedley TJ (1999) Michael James Lighthill (1924–1998). Notices AMS 46(1):1226–1229
2. Pedley TJ (2001) James Lighthill and his contributions to fluid mechanics. Annu Rev Fluid Mech 33:1–41
3. Lighthill MJ (1952) On sound generated aerodynamically, I. General theory. Proc R Soc Lond A 211:564–587

4. Crighton DG (1981) Acoustics as a branch of fluid mechanics. J Fluid Mech 106:261–298
5. Lighthill MJ (1954) On sound generated aerodynamically II. Turbulence as a source of sound. Proc R Soc Lond A 222:1–32
6. Lighthill MJ (1962) Sound generated aerodynamically, the Bakerian Lecture 1961. Proc R Soc Lond A 267:147–182
7. Lighthill MJ (1993) A general introduction to aeroacoustics and atmospheric sound. In: Hardin JC, Hussaini MY (eds) Computational Aeroacoustics. Springer-Verlag, New York
8. Stein RF (1967) Generation of acoustic and gravity waves by turbulence in an isothermal stratified atmosphere. Solar Phys 2:385–432
9. Crighton DG (1975) Basic principles of aerodynamic noise generation. Prog Aerosp Sci 16:13–96
10. Howe MS (2001) Vorticity and the theory of aerodynamic sound. J Eng Math 41(4):367–400
11. Crighton DG (1988) Aeronautical acoustics: mathematics applied to a major industrial problem. In: McKenna J, Temam R (eds) Proceedings of the first international conference on industrial and applied mathematics ICIAM'87. SIAM, Philadelphia, pp 75–89
12. Smith MJT (1989) Aircraft noise. Cambridge University Press
13. Lighthill MJ (1972) The propagation of sound through moving fluids, the fourth annual fairey lecture. J Sound Vibration 24:472–492
14. Swinbanks MA (1975) The sound field generated by a source distribution in a long duct carrying sheared flow. J Sound Vibration 40(1):51–76
15. Lighthill MJ (1965) Group velocity. J Inst Math Appl 1:1–28
16. Lighthill MJ (1960) Studies on magneto-hydrodynamic waves and other anisotropic wave motions. Phil Trans R Soc Lond A 252:397–430
17. Lighthill MJ (1978) Waves in fluids. Cambridge University Press
18. Rienstra SW (1999) Sound transmission in slowly varying circular and annular lined ducts with flow. J Fluid Mech 380:279–296
19. Rienstra SW (2003) Sound propagation in slowly varying lined flow ducts of arbitrary cross-section. J Fluid Mech 495:157–173
20. Rademaker ER (1990) Experimental validation of a lined-duct acoustics model including flow. Presented at ASME conference on duct acoustics, Dallas, TX, Nov. 1990
21. Ingard KU (1959) Influence of fluid motion past a plane boundary on sound reflection, absorption, and transmission. J Acoust Soc Am 31(7):1035–1036
22. Myers MK (1980) On the acoustic boundary condition in the presence of flow. J Sound Vibration 71(3):429–434
23. Eversman W, Beckemeyer RJ (1972) Transmission of sound in ducts with thin shear layers—convergence to the uniform flow case. J Acoust Soc Am 52(1):216–220
24. Rienstra SW (2003) A classification of duct modes based on surface waves. Wave Motion 37(2):119–135
25. Tester BJ (1973) The propagation and attenuation of sound in ducts containing uniform or 'Plug' flow. J Sound Vibration 28(2):151–203
26. Bers A, Briggs RJ (1963) MIT Research Laboratory of Electronics Report No. 71 (unpublished)
27. Briggs RJ (1964) Electron-stream interaction with plasmas. Monograph no. 29, MIT Press, Cambridge Massachusetts
28. Bers A (1983) Space-time evolution of plasma instabilities—absolute and convective. In: Galeev AA, Sudan RN (eds) Handbook of plasma physics: volume 1 basic plasma physics, Chapter 3.2. North Holland Publishing Company, pp 451–517
29. Crighton DG, Leppington FG (1974) Radiation properties of the semi-infinite vortex sheet: the initial-value problem. J Fluid Mech 64(2):393–414
30. Jones DS, Morgan JD (1972) The instability of a vortex sheet on a subsonic stream under acoustic radiation. Proc Camb Philos Soc 72:465–488
31. Quinn MC, Howe MS (1984) On the production and absorption of sound by lossless liners in the presence of mean flow. J Sound Vibration 97(1):1–9
32. Rienstra SW (1981) Sound diffraction at a trailing edge. J Fluid Mech 108:443–460
33. Koch W, Möhring W (1983) Eigensolutions for liners in uniform mean flow ducts. AIAA J 21:200–213
34. Daniels PG (1985) On the unsteady Kutta condition. Quar J Mech Appl Math 31:49–75
35. Goldstein ME (1981) The coupling between flow instabilities and incident disturbances at a leading edge. J Fluid Mech 104:217–246
36. Crighton DG, Innes D (1981) Analytical models for shear-layer feed-back cycles. AIAA81-0061, AIAA Aerospace Sciences Meeting, 19th, St. Louis, MO, 12–15 Jan. 1981
37. Brandes M, Ronneberger D (1995) Sound amplification in flow ducts lined with a periodic sequence of resonators. AIAA paper 95–126, 1st AIAA/CEAS Aeroacoustics Conference, Munich, Germany, 12–15 June 1995
38. Aurégan Y, Leroux M, Pagneux V (2005) Abnormal behavior of an acoustical liner with flow. Forum Acusticum 2005, Budapest
39. Munt RM (1977) The interaction of sound with a subsonic jet issuing from a semi-infinite cylindrical pipe. J Fluid Mech 83(4):609–640
40. Munt RM (1990) Acoustic radiation properties of a jet pipe with subsonic jet flow: I. The cold jet reflection coefficient. J Sound Vibration 142(3):413–436
41. Morgan JD (1974) The interaction of sound with a semi-infinite vortex sheet. Quart J Mech Appl Math 27:465–487
42. Bechert DW (1980) Sound absorption caused by vorticity shedding, demonstrated with a jet flow. J Sound Vibration 70:389–405
43. Bechert DW (1988) Excitation of instability waves in free shear layers. Part 1. Theory. J Fluid Mech 186:47–62
44. Howe MS (1979) Attenuation of sound in a low Mach number nozzle flow. J Fluid Mech 91:209–229
45. Cargill AM (1982) Low-frequency sound radiation and generation due to the interaction of unsteady flow with a jet pipe. J Fluid Mech 121:59–105
46. Cargill AM (1982) Low frequency acoustic radiation from a jet pipe—a second order theory. J Sound Vibration 83:339–354
47. Rienstra SW (1983) A small Strouhal number analysis for acoustic wave-jet flow-pipe interaction. J Sound Vibration 86:539–556

48. Rienstra SW (1984) Acoustic radiation from a semi-infinite annular duct in a uniform subsonic mean flow. J Sound Vibration 94(2):267–288
49. Crighton DG (1985) The Kutta condition in unsteady flow. Ann Rev Fluid Mech 17:411–445
50. Peters MCAM, Hirschberg A, Reijnen AJ, Wijnands APJ (1993) Damping and reflection coefficient measurements for an open pipe at low Mach and low Helmholtz numbers. J Fluid Mech 256:499–534
51. Cummings A (1983) Acoustic nonlinearities and power losses at orifices. AIAA J 22:786–792
52. Allam S, Åbom M (2006) Investigation of damping and radiation using full plane wave decomposition in ducts. J Sound Vibration 292:519–534
53. Michalke A (1965) On spatially growing disturbances in an inviscid shear layer. J Fluid Mech 23(3):521–544
54. Jones DS, Morgan JD (1974) A linear model of a finite Helmholtz instability. Proc R Soc Lond A 344:341–362
55. Noble B (1958) Methods based on the Wiener–Hopf technique. Pergamon Press, London
56. Heins AE, Feshbach H (1947) The coupling of two acoustical ducts. J Math Phys 26:143–155
57. Levine H, Schwinger J (1948) On the radiation of sound from an unflanged circular pipe. Phys Rev (APS) 73(4):383–406
58. Rienstra SW (1986) Hydrodynamic instabilities and surface waves in a flow over an impedance wall. In: Comte-Bellot G, Ffowcs Williams JE (eds) Proceedings IUTAM symposium 'aero- and hydro-acoustics' 1985 Lyon. Springer-Verlag, Heidelberg, pp 483–490
59. Abramowitz M, Stegun IA (1964) Handbook of mathematical functions. National Bureau of Standards, Dover Publications Inc., New York
60. Rienstra SW (2006) Impedance models in time domain, including the extended Helmholtz resonator model. AIAA Paper 2006-2686, 12th AIAA/CEAS Aeroacoustics Conference, 8–10 May 2006, Cambridge, MA, USA
61. Miles JW (1957) On the reflection of sound at an interface of relative motion. J Acoust Soc Am 29(2):226–228
62. Kelvin L (1871) Hydrokinetic solutions and observations. Philos Mag 4(42):362–377
63. von Helmholtz H (1868) On discontinuous movement of fluids. Philos Mag 4(36):337–346
64. Chevaugeon N, Remacle J-F, Gallez X (2006) Discontinuous Galerkin implementation of the extended Helmholtz resonator impedance model in time domain. AIAA paper 2006-2569, 12th AIAA/CEAS Aeroacoustics Conference, Cambridge, MA, 8–10 May 2006